Condensation and aggregation of solar corundum and corundum-hibonite grains

T. M. NAKAMURA[1], N. SUGIURA[1*], M. KIMURA[2], A. MIYAZAKI[1], and A. N. KROT[3]

[1]Department of Earth and Planetary Science, University of Tokyo, Tokyo, Japan
[2]Faculty of Science, Ibaraki University, Mito, Japan
[3]Hawai'i Institute of Earth and Planetary Science, School of Ocean, Earth Science and Technology,
University of Hawai'i at Manoa, Honolulu, Hawai'i 96822, USA
*Corresponding author. E-mail: sugiura@eps.s.u-tokyo.ac.jp

Abstract–Forty-three corundum grains (1–11 μm in size) and 5 corundum-hibonite grains with corundum overgrown by hibonite (4–7 μm in size), were found in the matrix of the mineralogically pristine, ungrouped carbonaceous chondrite Acfer 094 by using cathodoluminescence imaging. Some of the corundum and corundum-hibonite grains occur as aggregates of 2 to 6 grains having similar sizes. The oxygen isotopic compositions of some of the corundum-bearing grains suggest their solar nebula origin. ^{26}Al-^{26}Mg systematics of one corundum grain showed the canonical initial $^{26}Al/^{27}Al$ ratio, also suggesting a solar nebula origin. Quantitative evaluation of condensation and accretion processes made based on the homogeneous nucleation of corundum, diffusion-controlled hibonite formation, collisions of grains in the nebula, and critical velocity for sticking, indicates that, in contrast to the hibonite-bearing aggregates of corundum grains, the hibonite-free corundum aggregates could not have formed in the slowly cooling nebular region with solar composition. We suggest instead that such aggregates formed near the protosun, either in a region that stayed above the condensation temperature of hibonite for a long time or in a chemically fractionated, Ca-depleted region, and were subsequently physically removed from this hot region, e.g., by disk wind.

INTRODUCTION

Equilibrium condensation calculations for a cooling gas of solar composition at a total pressure of $<10^{-2}$ atm show that corundum (Al_2O_3) should be the first major condensate (Yoneda and Grossman 1995; Ebel 2006). With continued cooling, corundum condensates are predicted to react with the nebular gas to form hibonite ($CaAl_{12}O_{19}$). Apparently, in many cases it did, because hibonite-bearing Ca-Al-rich inclusions (CAIs) are much more abundant than corundum-bearing ones (Simon et al. 2002). Only eleven corundum-bearing CAIs have been previously described in detail. These include M98-8, BB-5, and GR-1 from the CM carbonaceous chondrite Murchison (Simon et al. 2002; Bar-Matthews et al. 1982; MacPherson et al. 1984a; Hinton et al. 1988), F5 from the CM chondrite Murray (Fahey 1988), #32 and #50 from the ungrouped carbonaceous chondrite Adelaide (Krot at al. 2001), s2 from the ungrouped carbonaceous chondrite Acfer 094 (Krot at al. 2004), and S159A41, S159B36, S159B34, and S159B43 from the EH chondrite Sahara 97159 (Lin et al. 2003). Some of these CAIs are considered to be direct condensates from the solar nebula gas, whereas others may have experienced subsequent melting and/or evaporation. In addition to the corundum-bearing CAIs, micrometer-size corundum grains are commonly found in acid-resistant residues of primitive ordinary, enstatite, and carbonaceous chondrites. Only a few of these grains have presolar origin; most grains appear to have formed in the early solar system (e.g., Nittler 1997; Zinner 2003 and references therein). High-temperature condensation processes in the solar nebula can be potentially elucidated from studies of the solar, corundum-bearing grains. Ten small (500 nm to 5 μm) corundum grains of solar origin have been previously reported in the matrix of LL3.1 ordinary chondrite Krymka (Strebel et al. 2001), but no petrographic information was provided. Using time-of-flight secondary ion mass spectrometry (TOF-SIMS) and NanoSIMS, Bland et al. (2005, 2007) studied in situ three small (<5 μm) corundum-bearing inclusions in the Acfer 094 matrix and observed 200–300 nm hibonite overgrowths on all of them. Two of these inclusions have ^{16}O-poor isotopic compositions ($\delta^{17}O = 11 \pm 12‰$ and $-2 \pm 4‰$, $\delta^{18}O = 6 \pm 5‰$, and $6 \pm 3‰$, respectively), another inclusion is ^{16}O-rich ($\delta^{17}O = -28 \pm 3‰$, $\delta^{18}O = -29 \pm 1‰$). All data are normalized to the Acfer 094 matrix.

Acfer 094 is an ungrouped carbonaceous chondrite with mineralogical, petrographic, nitrogen isotopic, and oxygen isotopic affinities to the CM and CO chondrites (Newton et al. 1995; Greshake 1997). While its matrix mineralogy and bulk oxygen isotopic composition of Acfer 094 imply affinities to CO chondrites, its bulk chemical composition and trace element abundances are similar to those of CM chondrites (Wlotzka 1991; Spettel et al. 1992). Bischoff and Geiger (1994) suggested that Acfer 094 might be the first CM3 chondrite. However, this is not supported by its bulk carbon and nitrogen isotopic compositions (Newton et al. 1995). Acfer 094 largely escaped thermal metamorphism and aqueous alteration; it contains only minor amounts of serpentine and ferrihydrite in the matrix (Greshake 1997). Furthermore, Grossman and Brearley (2005) showed that chemical features of olivine in Acfer 094 are indicative of a very low grade of thermal metamorphism. Kimura et al. (2006) indicated that Fe-Ni metals in Acfer 094 are mainly martensite and were not subjected to thermal metamorphism. Acfer 094 contains the highest abundance of presolar SiC compared to any other meteorite studied so far (Newton et al. 1995; Gao et al. 1996), and high abundances of presolar silicates have been recently reported as well (Nguyen and Zinner 2004; Nagashima et al. 2004; Mostefaoui and Hoppe 2004). Based on these observations, we infer that Acfer 094 should also contain pristine solar nebula materials, including high-temperature gas-solid condensates, such as corundum and hibonite. This is supported by the presence of the mineralogically pristine refractory inclusions in Acfer 094 described by Krot et al. (2004).

Here we report an in situ discovery of 43 corundum grains (1–11 μm in size) and 5 corundum-hibonite (corundum overgrown by hibonite) grains (4–7 μm in size) in the Acfer 094 matrix using cathodoluminescence. The textures, chemical compositions, oxygen isotopic compositions, and ^{26}Al-^{26}Mg systematics of the corundum-bearing grains were investigated. Some of the corundum and corundum-hibonite grains occur as aggregates. The environment in which these aggregates formed was studied based on quantitative analyses of condensation and aggregation processes. Preliminary results of this study have been previously reported by Nakamura et al. (2005, 2006).

ANALYTICAL TECHNIQUES

To detect corundum-bearing grains, two carbon-coated, polished thin sections of Acfer 094, #1 and #2, with surface areas of ~34 mm^2 and ~170 mm^2, respectively, were examined by cathodoluminescence (CL) imaging, backscattered electron (BEI), and secondary electron imaging (SEI) using a JEOL JMS-5310 scanning electron microscope (SEM) equipped with the CL detector (Mini CL, Gatan Inc.), as well as by energy dispersive X-ray spectrometer (EDX) at the University of Tokyo. To avoid contamination by Al$_2$O$_3$ of the polishing compound, the thin sections were prepared using only diamond pastes. The SEM was operated using a 0.5 nA beam current at 20 kV accelerating voltage. Identification of mineral phases was made mainly based on the EDX measurements. Corundum grains were searched using CL images at a magnification of 200 times. Since corundum is the brightest mineral in CL images, corundum grains ~1 μm in diameter, corresponding approximately to a pixel size of the CL image at this magnification, can be detected. Detection of corundum grains of smaller sizes using CL is less efficient because of a weaker CL signal. The detected corundum grains were studied in BSE mode and by EDX. Some of the corundum grains were found to be overgrown by hibonite. Quantitative electron microprobe analyses (EPMA) of one corundum grain (#2-11) and three corundum-hibonite grains (#2-17, #2-23, and #2-26) were performed with a JEOL 733 electron microprobe at the Ibaraki University. Other grains were too small to obtain quantitative compositional data. EPMA analyses were conducted generally at 15 kV and a sample current of 20 nA. The X-ray overlaps of K$_\alpha$ on K$_\beta$ lines of some successive elements were corrected with a deconvolution program. The Bence-Albee matrix correction method was used. The detection limits (3σ, in wt%) are 0.03 for Al$_2$O$_3$, MgO, and CaO, 0.05 for SiO$_2$, TiO$_2$, V$_2$O$_3$, and Cr$_2$O$_3$, 0.09 for FeO, NiO, and MnO.

To map the distribution of chondrules, refractory inclusions, and matrix, and to clarify the location of the corundum-bearing grains detected, both sections were mapped in Ca, Al, Mg, Si, and Ti K$_\alpha$ X-rays using a fully focused electron beam, 15 kV accelerating voltage, 100 nA beam current, 20–30 ms per pixel acquisition time, and resolution of ~8–10 μm per pixel with WDS detectors on a Cameca SX-50 electron microprobe at the University of Hawai'i. Seven corundum grains were studied by oxygen ion imaging using a resistive anode encoder attached to a Cameca IMS-6f ion microprobe at the University of Tokyo. For oxygen ion imaging, two Cs$^+$ primary beams with intensities different by a factor of ~500 were used. A weaker beam was used for ^{16}O imaging, whereas a stronger beam was used for ^{17}O, ^{18}O, and ^{27}Al imaging. The ^{16}O and ^{18}O count rates were approximately 2×10^4 counts per second. The mapped area by ion imaging corresponds to a circle ~30 μm in diameter. The entrance and exit slits were narrowed enough to eliminate the contribution of interfering ^{16}OH ions to the ^{17}O images. A normal incidence electron gun was used for charge compensation. The spatial resolution is better than 1 μm. Details of the ion imaging were explained by Sugiura (1998). The oxygen isotopic compositions of corundum were normalized to those of the Acfer 094 matrix reported by Nagashima et al. (2004).

Magnesium isotopic compositions of one corundum grain were measured using a Cameca IMS-6f. A 12.7 kV O$^-$ primary ion beam, ~7 μm in diameter, with an intensity

of 0.42 nA was used for sputtering. Positive secondary ions of Mg and Al were accelerated at 10.0 kV. A Faraday cup was used to detect $^{27}Al^+$ and 26.9 amu (Faraday cup background), and $^{24}Mg^+$, $^{25}Mg^+$, and $^{26}Mg^+$ were detected with an electron multiplier. Mass resolving power was set to about 4500.

Electron backscattered diffraction (EBSD) was used to obtain crystallographic information of five corundum grains forming an aggregate. The sample studied by EBSD was polished with colloidal silica. EBSD images were taken using a JEOL 7000F field emission SEM with the Channel 5 software package of HKL Tech. Inc. The electron accelerating voltage was 15 kV and the beam current was 2 nA.

RESULTS

Abundance of Corundum Grains in Matrix of Acfer 094 and Their Size Distribution

Using CL and EDX analyses, 43 corundum and 5 corundum-hibonite grains were identified in the Acfer 094 matrix; no corundum grains were found inside chondrules or refractory inclusions (except for the one reported by Krot et al. [2004]). The corundum and corundum-hibonite grains or their aggregates occur as individual objects and are not associated with minerals commonly observed in CAIs, such as melilite, spinel, Al-Ti-diopside, or perovskite. Based on the surface areas of the corundum-bearing grains and the studied matrix, the abundance of corundum grains in the Acfer 094 matrix, which corresponds to ~35 vol% of the meteorite (Newton et al. 1995), is estimated to be ~8 ppm. This is similar to the abundance (~6 ppm) of corundum grains in the Krymka (LL3.1) matrix (Strebel et al. 2001).

The apparent size distribution of the corundum-bearing grains exposed in polished surfaces of Acfer 094 is shown in Fig. 1. For a rounded grain, the size corresponds to its diameter; for other grains, the size corresponds to a diameter of a circle with an equivalent cross section area. The corundum grains range in size from 1 to 11 μm, with a typical size of ~2 μm. The corundum-hibonite grains range in size from 4 μm to 7 μm and are generally larger than the average size of corundum grains. The texture of a corundum core surrounded by a hibonite mantle (Figs. 2c and 2f) suggests that they formed by condensation rather than by evaporation. No corundum-bearing grains smaller than 1 μm were detected, probably because of poor detection efficiency for such grains. Bland et al. (2005) reported much smaller corundum-bearing grains in Acfer 094 using TOF-SIMS. It may be worth noting, however, that the typical size of corundum grains in Krymka (LL3.1) is ~1–2 μm (Strebel et al. 2001), quite similar to that shown in Fig. 1. More CL observations at higher magnifications are needed to establish the corundum size distribution.
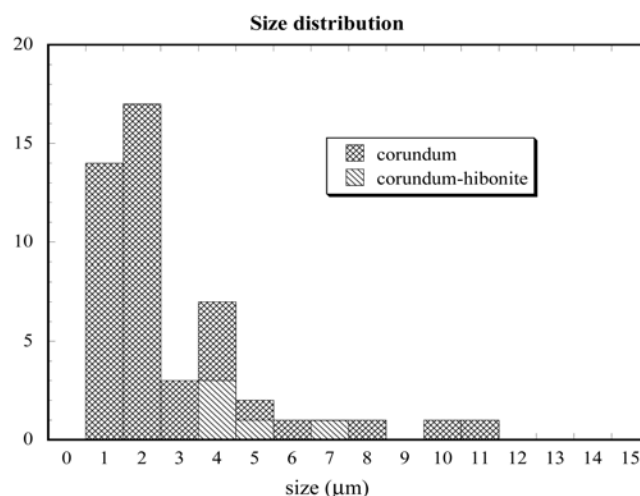

Fig. 1. Apparent size distributions of corundum and corundum-hibonite grains in polished sections of Acfer 094 matrix.

Corundum-Bearing Aggregates

Some of the corundum-bearing grains occur as aggregates. Six aggregates were found, each consisting of two to six grains of similar sizes. Figures 2a and 2b show the hibonite-free corundum aggregates #2-25 and #2-11 consisting of five and six grains, respectively. Figure 2c shows aggregate #2-23 consisting of three corundum grains, each overgrown by a hibonite. No mixed aggregates composed of both corundum and corundum-hibonite grains were observed. Although the grains exposed on the surface of the thin section are separated by a thin layer of matrix material, the similar mineralogy and sizes of the grains suggest that they are probably connected in three-dimensional space. The corundum-bearing aggregates show various degrees of sintering (e.g., compare #2-11 and #2-23).

Mineral Chemistry

Because of the small grain sizes, accurate determination of chemical compositions of the corundum and corundum-hibonite grains using EPMA is difficult in many cases. Nevertheless, we obtained reliable data for relatively large grains (Table 1). Analyses of the corundum grains in aggregate #2-11 indicate that they are almost pure Al_2O_3. Corundum grains in #2-11 contain less CaO and TiO_2 than the corundum grains from CAIs (GR-1: MacPherson et al. 1984a; BB-5: Bar-Matthews et al. 1982; M98-8: Simon et al. 2002; #50: Krot et al. 2001).

Analyses of the corundum-bearing grains #2-23 and #2-26 confirmed that corundum is overgrown by hibonite. The hibonite overgrowths contain lower TiO_2 and MgO (<0.08 and 0.06–0.08 wt%, respectively) and higher FeO (>1 wt%) compared with hibonites of the corundum-bearing CAIs reported by Simon et al. (2002) and Krot et al. (2001).
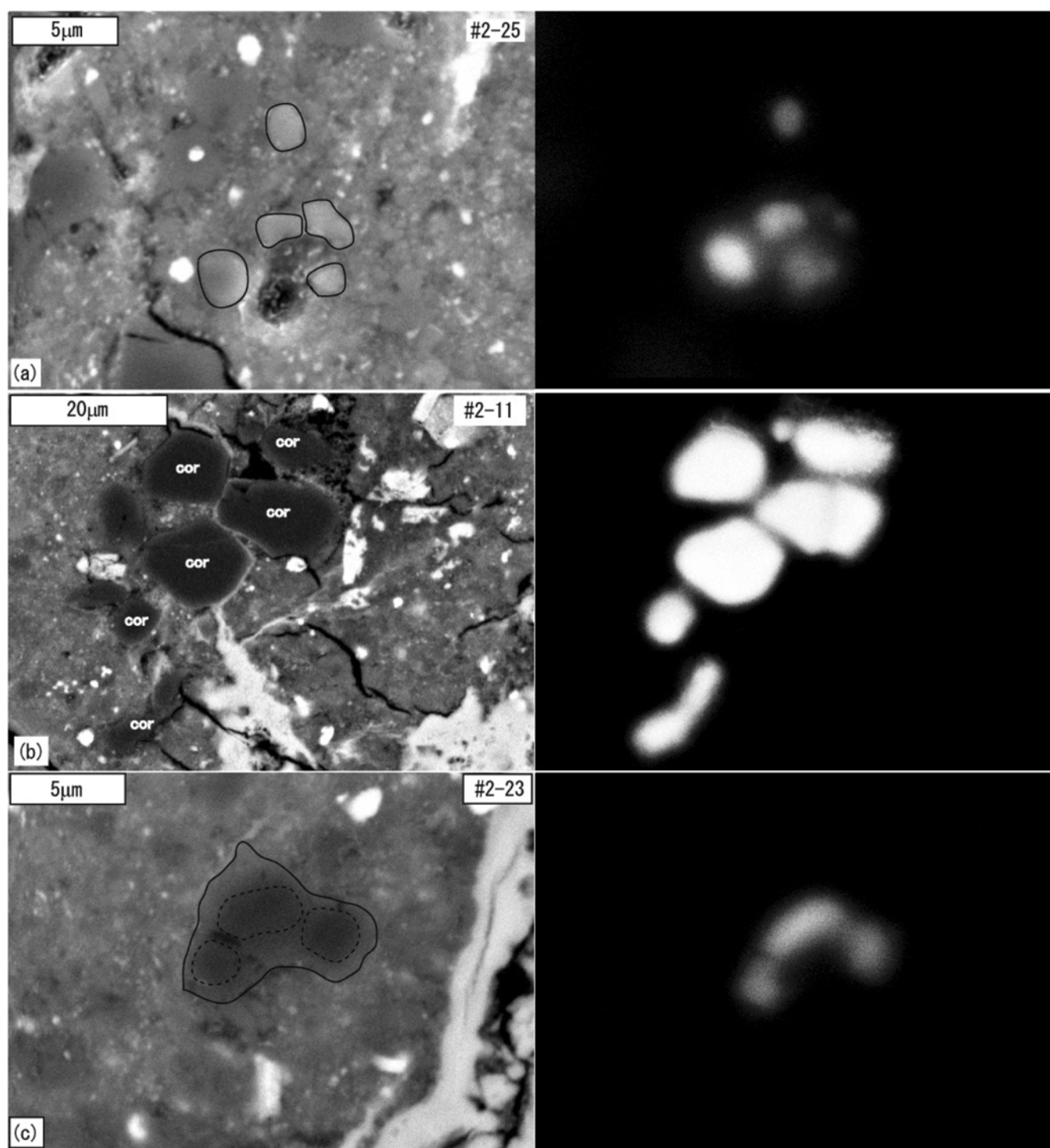
Fig. 2. Paired electron microscope and CL images of the same field of view of corundum and corundum-hibonite grains in the Acfer 094 matrix. Corundum is luminescent; hibonite is non-luminescent. The microscope image of (a) is a secondary electron image, whereas those of (b–f) are backscattered electron images. a) Aggregate #2-25 of five corundum grains that are outlined in the secondary electron image. Two grains on the right are faint in the CL image and the positions in the CL image are slightly offset from those of the secondary ion image. They may be located below the surface. b) Aggregate #2-11 of six corundum grains. They are marked with "cor" in the backscattered electron image. c) Aggregate #2-23 of three corundum grains overgrown by hibonite. The hibonite is outlined by a solid curve; three corundum grains are outlined by broken curves.
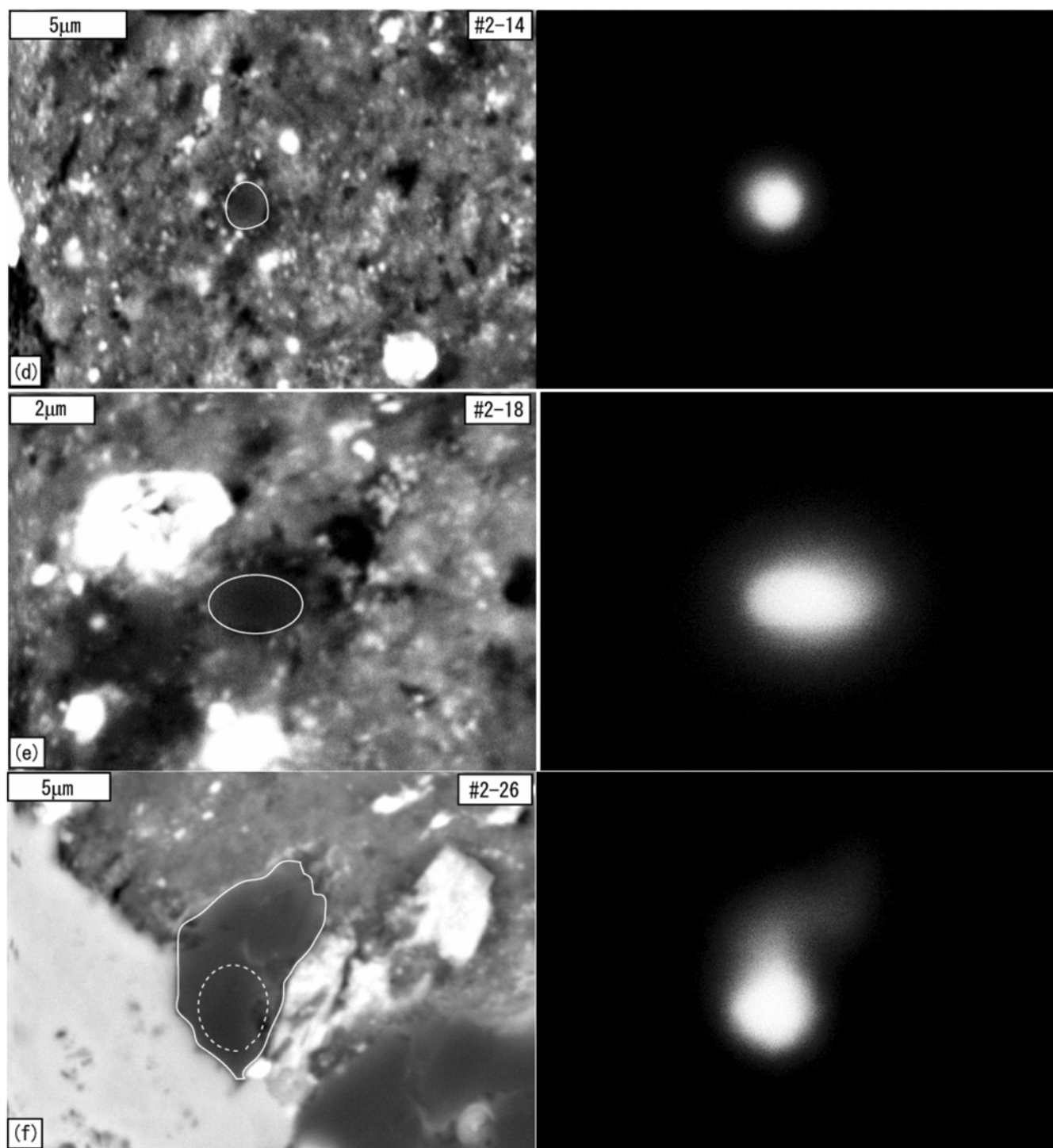
Fig. 2. *Continued.* d) and e) Isolated corundum grains #2-14 and #2-18, respectively. f) Isolated corundum grain #2-26 with a thick hibonite overgrowth. The hibonite is outlined by a solid curve; the corundum core is outlined by a broken curve. A faint tail in the CL image suggests that the corundum extends toward the upper right below the surface hibonite.

Table 1. Selected analytical data of corundum and hibonite.

	Phase	SiO_2	TiO_2	Al_2O_3	FeO	MgO	CaO	Total
#2-11	Corundum	b.d.	0.09	98.64	0.58	b.d.	b.d.	99.31
#2-23	Corundum	0.29	b.d.	96.04	1.06	0.07	0.37	97.83
#2-26	Corundum	0.52	b.d.	96.22	1.75	0.15	0.10	98.74
#2-23	Hibonite	0.19	0.08	87.75	1.08	0.06	7.70	96.86
#2-26	Hibonite	b.d.	b.d.	90.81	1.16	0.08	8.33	100.38

b.d. = below detection limits. Cr, V, Ni, and Mn were below detection limits for all the corundum-bearing objects.

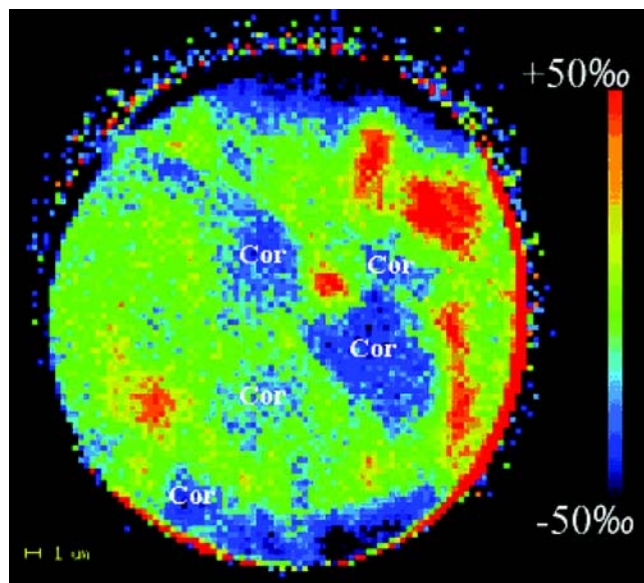Fig. 3. Oxygen ion image ($^{18}O/^{16}O$) of five corundum grains (marked as Cor) in the aggregate #2-11 (see Fig. 2b); another corundum grain of the aggregate is outside the field of view. The scale bar shows $\delta^{18}O$ ranging from +50‰ (red) to –50‰ (blue). The isotopic compositions are not accurate near the edge due to an aberration in the imaging system. Red regions correspond to FeS. This apparent positive anomaly in $\delta^{18}O$ is probably due to interference of multiply charged complex molecules made of sulfur and hydrogen.

High FeO contents are probably due to small sizes of the hibonite grains and excitation of the surrounding matrix material by the electron beam during the analyses. Furthermore, most of the Mg signal probably comes from the matrix material because the TiO_2/MgO ratios are much smaller than expected for hibonite.

Oxygen Ion Imaging

Figure 3 shows a quantitative ion image in $\delta^{18}O$ of the corundum aggregate #2-11. Five corundum grains can be recognized by their bluish color. The red regions in the matrix correspond to FeS; the apparent positive anomaly in $\delta^{18}O$ is probably due to interference of multiply charged complex molecules made of sulfur and hydrogen. Although slight variations in the $\delta^{18}O$ of the corundum grains may be also partly due to unidentified interferences, these grains have $\delta^{18}O$ values as low as –50‰, which is similar to those of CAIs. Hence, these corundum grains are unlikely to be the presolar grains or products of terrestrial contamination. The oxygen isotope compositions of five corundum grains and one corundum-hibonite aggregate (not shown), although of poorer quality because of smaller sizes, are similar to those shown in Fig. 3. Ion images of $\delta^{17}O$ (not shown) are similar to those of $\delta^{18}O$ but of lower quality due to poor counting statistics. Our results are consistent with those reported by Strebel et al. (2001) for Krymka corundum grains.

Al-Mg Isotope Systematics

One corundum grain of aggregate #2-11 analyzed for Mg isotopic compositions revealed significant ^{26}Mg excesses (Fig. 4). Since no grains with low Al/Mg ratios occur in the aggregate, we assumed that the Al-Mg isochron passes through the origin of the isochron diagram. The inferred initial $^{26}Al/^{27}Al$ ratio is $(5.8 \pm 1.2) \times 10^{-5}$, indistinguishable from the canonical and supracanonical values of 5×10^{-5} (MacPherson et al. 1995) and $(5.85 \pm 0.05) \times 10^{-5}$ (Thrane et al. 2006), respectively. Other corundum-bearing grains were too small to make precise determination of the initial $^{26}Al/^{27}Al$ ratios.

EBSD Analysis

Figure 5 shows EBSD mapping of the corundum aggregate #2-11 acquired with the spatial resolution of ~0.5 μm. Different colors indicate different crystal orientations. Deviation in the crystal orientation within a corundum grain determined by EBSD is typically less than 1 degree. Differences in the crystal orientations between the grains are of the order of tens of degrees. Therefore, there is practically no ambiguity in the interpretation of EBSD results. Four out of five corundum grains are single crystals. The remaining grain consists of two crystals that are shown in pink and green.

DISCUSSION

Constraints on the Environment of the Corundum-Forming Region of the Solar Nebula

Based on the Al-Mg systematics measured for one corundum aggregate and oxygen isotopic compositions of seven corundum-bearing grains measured in the Acfer 094 matrix, we conclude that these grains formed in the early solar
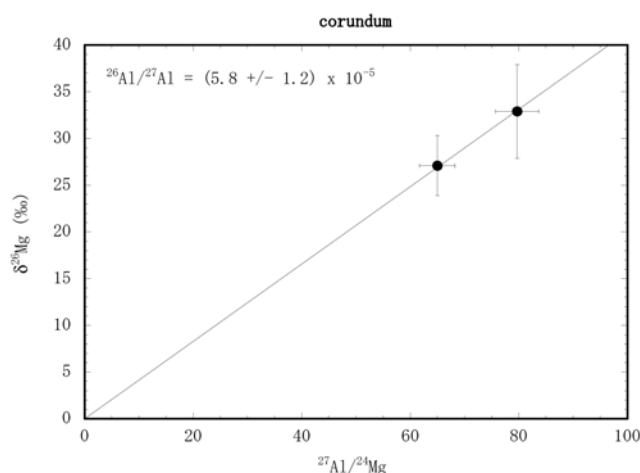
Fig. 4. Isochron diagram for a corundum grain in the corundum aggregate #2-11. The initial $^{26}Al/^{27}Al$ ratio was estimated assuming that the isochron passes through the origin. The error of the initial ratio is 2σ.
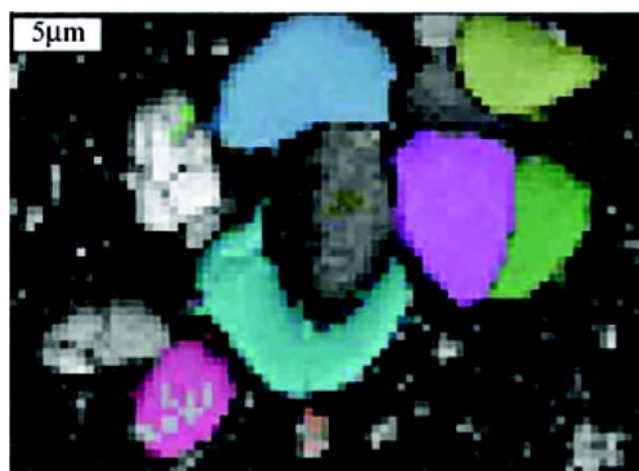

Fig. 5. EBSD map of five corundum grains in the aggregate #2-11 (see Fig. 2b). Different colors indicate different crystal orientations. Four out of five grains are single crystals; the remaining grain consists of two pink and green subgrains. The central gray area is a crater produced by previous SIMS measurements and did not give an adequate signal for the EBSD analysis.

system, most likely in the CAI-forming region. Based on the sizes of the corundum grains (1–11 μm), the presence or absence of hibonite overgrowths and their thicknesses, and the existence of the corundum ± hibonite aggregates and their textures, we can put some constraints on their formation environment.

The presence of hibonite overgrowths around the corundum grains in aggregate #2-23 and its well-sintered (annealed) texture (Fig. 2c) may indicate a long residence time of the aggregate or individual corundum grains prior to their aggregation in the slowly cooling nebular region of their formation that allowed continued reaction of corundum condensates with gaseous calcium. Since direct condensation of Al and Ca from gas constitutes a very small fraction of hibonite, and since the expected volume increase for conversion of corundum to hibonite is also small, hibonite grain shape should closely follow the shape of pre-existing corundum grains. Therefore, unless corundum grains had been well-sintered, sintering has to occur after the start of hibonite formation. The absence of lower temperature condensates, such as perovskite, melilite, spinel, and Al,Ti-diopside, associated with the hibonite-corundum grains or their aggregates, suggests that the corundum-bearing grains were chemically isolated, either physically or by kinetic effects from subsequent reactions with the cooling nebular gas.

Aggregate #2-11 of six relatively large (~10 μm) corundum grains (these are the largest corundum grains detected in this study) appears to contain no hibonite overgrowths (Fig. 2b). Backscattered electron, CL (Fig. 2b), and EBSD (Fig. 5) images suggest that if hibonite overgrowth is present, its thickness is below the resolution limits. This observation can be interpreted as evidence for very slow cooling of the nebular region during the growth of the

corundum grains followed by a sudden drop in temperature or fast removal of these grains from this region to avoid formation of hibonite overgrowths. The corundum grains are poorly sintered (with a possible exception of a polycrystal made of two subgrains, see Fig. 2b and Fig. 5), which is consistent with rapid cooling after aggregation.

Below, we attempted to quantify physico-chemical conditions of the nebular region where the corundum-bearing grains (#2-11 and #2-23) condensed and aggregated.

Grain Size and Cooling Time According to a Homogeneous Nucleation Theory

The equilibrium condensation temperature (T_e) of corundum from a gas of solar composition at total pressures 10^{-6} (1571 K) to 10^{-3} atm (1770 K) is slightly higher than that of hibonite (1485 and 1743 K, respectively) (e.g., Yoneda and Grossman 1995; Ebel and Grossman 2000; Ebel 2006). However, formation of corundum in the absence of solid precursors (i.e., from temperatures above T_e) requires the formation of condensation nuclei, i.e., homogeneous condensation. In the case of homogeneous condensation, the actual condensation temperature of corundum (T_c) is lower than that predicted by the equilibrium condensation theory (Blander and Katz 1967). In the following discussion, we assume that corundum grains formed by homogeneous condensation. In contrast, condensation of hibonite rims around corundum grains occur by heterogeneous condensation as a result of reaction between the earlier formed corundum and nebular gas at temperatures close to the equilibrium condensation temperature of hibonite because much less energy is required for forming condensation nuclei.
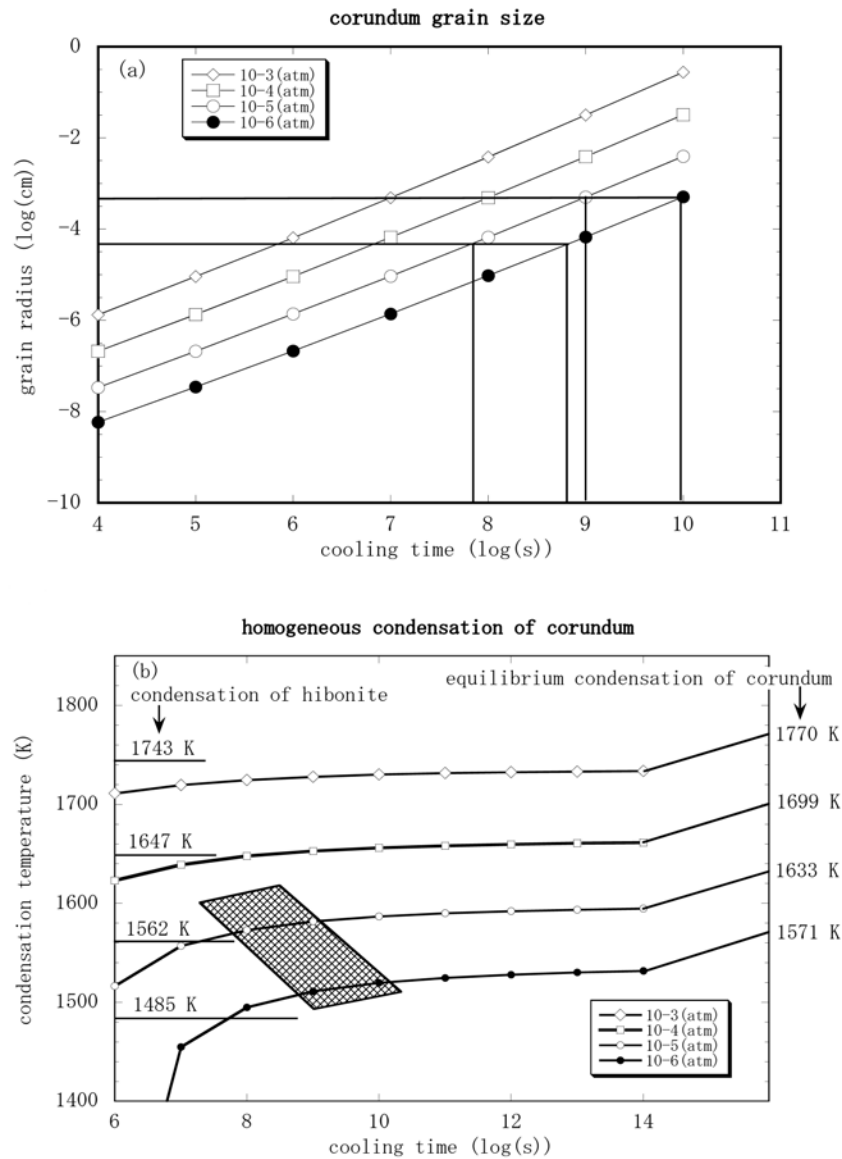
Fig. 6. a) Corundum grain radius as a function of cooling time of the solar nebula region where they formed and total pressure ranging from 10^{-3} to 10^{-6} atm (based on Figs. 1 and 2 of Kozasa and Hasegawa 1987). Cooling times corresponding to the formation of the 1 μm and 10 μm size grains at 10^{-5} and 10^{-6} atm are shown by thick lines. b) Condensation temperature of corundum as a function of cooling time of the solar nebula region where it formed and total pressures ranging from 10^{-3} to 10^{-6} atm (based on Kozasa and Hasegawa 1987). Equilibrium condensation temperatures of corundum and hibonite (Yoneda and Grossman 1995) are shown for comparison along the right and left vertical axes, respectively. Cross-hatched area shows the possible range of cooling times and pressures in the formation region of 1 to 10 μm size corundum grains.

According to a homogeneous nucleation theory (Kozasa and Hasegawa 1987), grain sizes of condensates are determined by cooling time $\tau = |dln(T)/dt|^{-1}$ and total pressure (P_t). In a cooling gas of solar composition, the predicted radii of corundum condensates are illustrated in Fig. 6a (reproduced from Kozasa and Hasegawa [1987]) as a function of τ and P_t.

From the sizes of the Acfer 094 corundum grains, the cooling time of the solar nebular region where they formed or the cooling rate, which is inversely proportional to the cooling

time, can be calculated as a function of P_t (Fig. 6a). The total pressure of the nebular gas is generally assumed to be in the range from 10^{-6} to 10^{-3} atm (e.g., Ebel and Grossman 2000). As will be discussed below, at P_t higher than $\sim 3 \times 10^{-5}$ atm, the homogeneous condensation temperature of corundum is lower than the condensation temperature of hibonite. Since our petrographic observations clearly indicate that corundum in the Acfer 094 matrix predates formation of hibonite (see also Bland et al. 2005), in the framework of the homogeneous condensation theory, P_t has to be lower than $\sim 3 \times 10^{-5}$ atm.

Cooling times for a 1 μm size corundum grain at 10^{-6} and 10^{-5} atm are ~7×10^8 and ~7×10^7 s (22 and 2.2 yr), respectively. Cooling times for a 10 μm size corundum grain at 10^{-6} and 10^{-5} atm are ~1×10^{10} and ~1×10^9 s, respectively. The estimated cooling rates of the coarse-grained, igneous type B CAIs from the CV carbonaceous chondrites during their crystallization (i.e., from their liquidus temperatures (1550–1500 °C) to solidus temperatures) are 0.5–50 °C/hr (e.g., MacPherson et al. 1984b), which correspond to cooling times of 10^5–10^7 s. Therefore, the estimated cooling times for the corundum condensates are longer than those during crystallization of type B CAIs. A possible explanation for the slower cooling rates of the corundum grains could be additional, continuous heating due to solar irradiation. Because corundum is the highest temperature condensate from a gas of solar composition (e.g., Yoneda and Grossman 1995), it is expected to be the main constituent of the dust wall that is postulated to have been present at the innermost edge of the protoplanetary disk (Muzerolle et al. 2004). Since the inner edge of the dust wall made of corundum grains is expected to be transparent to solar radiation (the abundance of corundum grains condensing from a gas of solar composition is expected to be very low), it could keep corundum grains hot for a long period of time.

Homogeneous Condensation Temperature of Corundum

The difference between the equilibrium condensation temperature (T_e) and the homogeneous condensation temperature (T_c) of a condensate is mainly controlled by its surface energy (Kozasa and Hasegawa 1987; Blander and Katz 1967). Using the numerical constants given by Kozasa and Hasegawa (1987), the homogeneous condensation temperature of corundum was calculated as a function of total pressure and cooling time (Fig. 6b). At pressure higher than a few times 10^{-5} atm and with a cooling time estimated from the sizes of the Acfer 094 corundum grains (Fig. 6a), the homogeneous condensation temperature of corundum is lower than the equilibrium condensation temperature of hibonite. This means that corundum is expected to be replaced by hibonite as soon as it condenses, which is inconsistent with the presence of corundum. As a result, in the following discussion, the total pressure in the formation region of solar corundum grains is restricted to be less than a few times 10^{-5} atm.

Supporting evidence for the origin of the Acfer 094 corundum grains by homogeneous nucleation is similar sizes of individual corundum grains in an aggregate (Figs. 2a–c). It is known that homogeneous nucleation results in a narrow range of grain sizes. This is because once the condensation starts, formation of condensation nuclei ceases quickly due to decrease in the degree of supersaturation. In other words, grains grow quickly in a very narrow temperature range, resulting in a narrow range in grain size. In addition, the observed size range of corundum grains (1–10 μm) and the

presence of hibonite overgrowths around some of them suggest that these grains are condensates rather than evaporation residues. We note that some hibonites described in the literature, whose sizes are as large as 100 μm, and which often show nuclear isotopic anomalies and mass-dependent isotopic fractionation effects (e.g., platy hibonites in CM chondrites and hibonites in FUN CAIs), could have formed as evaporative residues (e.g., Ireland 1988). Although evaporation of such hibonite grains could have produced corundum residues, the latter are expected to have significantly larger size range (up to several tens of microns) than the corundum grains in Acfer 094. This is because evaporation of calcium and oxygen from hibonite to produce corundum results in only ~8% reduction in mass. Based on these observations, we infer that corundum grains in the Acfer 094 matrix formed as homogeneously nucleated condensates.

Time Scale of Formation of Hibonite Overgrowths

The presence of corundum grains and aggregates of grains without observable hibonite overgrowths (e.g., #2-11 shown in Fig. 2b) suggests that these corundum grains aggregated prior to formation of hibonite. Since hibonite overgrowths were undetectable by SEM (no transmission electron microscope study has been done so far), the hibonite overgrowths, if present, are assumed to be less than 0.1 μm thick. (This is an order of magnitude estimate. Hibonite overgrowth of ~0.5 μm thickness was observable on an aggregate #2-23. Hence the thickness of unobservable hibonite growth on #2-11 was assumed to be 0.1 μm.) Assuming that a nebular region with a solar bulk chemical composition cooled at a steady rate, we can estimate the time scale for the formation of hibonite overgrowths by reaction of corundum grains with the nebular gas. This time scale is a sum of τ_1, τ_2, and τ_3, where τ_1 is the time elapsed during cooling of the system from the homogeneous nucleation temperature of corundum to the equilibrium condensation temperature of hibonite, τ_2 is the time required for accumulation of calcium atoms on the corundum surface that is sufficient for the formation of a hibonite overgrowth, and τ_3 is the time required for the formation of hibonite assuming that it is controlled by calcium diffusion into corundum.

Time scale τ_1 can be estimated by considering the difference in the condensation temperatures of corundum and hibonite and the estimated cooling rates (which depend on the total pressure and the grain size) (Fig. 6a) based on the homogeneous nucleation theory. For a corundum grain 1 μm in size, the estimated τ_1 values are 8.6×10^6 and 1.5×10^5 sec at 10^{-6} and 10^{-5} atm, respectively (as discussed above, formation of the Acfer 094 corundum grains at higher pressures is inconsistent with petrographic observations). For a corundum grain 10 μm in size, the estimated τ_1 values are 1.9×10^8 and 8.6×10^6 s at 10^{-6} atm and 10^{-5} atm, respectively.
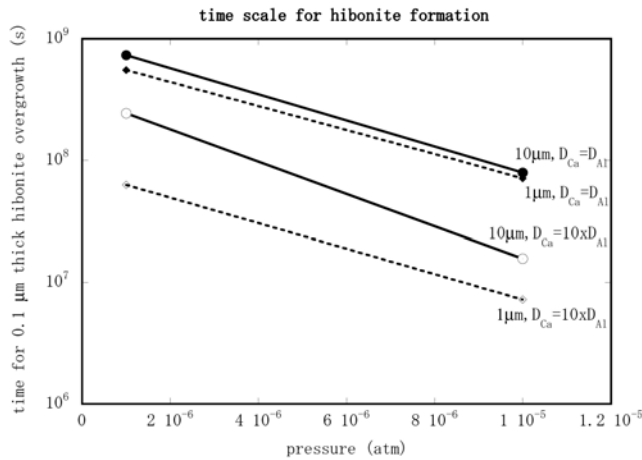
Fig. 7. Time for formation of 0.1 μm thick hibonite overgrowth. In cases of slow Ca diffusion ($D_{Ca} = D_{Al}$), the time scale is determined by Ca diffusion in 1 μm and 10 μm size corundum grains. With a fast Ca diffusion rate ($D_{Ca} = 10 \times D_{Al}$), the cooling time from the corundum homogeneous nucleation condensation temperature to hibonite equilibrium condensation temperature becomes the dominant factor for 10 μm size grains because of the slow cooling rate. The pressure dependence of the logarithm of the time for hibonite formation is not exactly linear, but the dependence is nearly linear and hence shown as a straight line.

Time scale τ_2 can be estimated based on the kinetic theory of an ideal gas. The condensation coefficient of calcium atoms on corundum (the probability of an incoming gas molecule to remain on the surface) is assumed to be 1. The mean time between two collisions of calcium atoms on a corundum grain can be expressed as $\tau_{Ca} = (n_{Ca} \sigma V_{Ca})^{-1}$, where n_{Ca} is the number density of calcium atoms in the gas phase that is proportional to the total pressure and the solar abundance of calcium, and σ and V_{Ca} are the cross section and the thermal velocity of calcium atoms, respectively. The number of aluminum atoms contained in a surface layer dr of a corundum grain with a radius r can be expressed as $N_{Al} = 2N_{Av}4\pi r^2 dr/M_{Al_2O_3}$, where $M_{Al_2O_3}$ is the mole weight of Al_2O_3 and N_{Av} is Avogadro's number. The chemical formula of pure hibonite is $CaAl_{12}O_{19}$; as a result, the number of calcium atoms needed for formation of a hibonite overgrowth is one-twelfth the number of aluminum atoms in an equal number of moles of corundum, $\tau_2 = \tau_{Ca}N_{Al}/12$. Because τ_2 is much smaller than τ_1 and τ_3 (see below), even if the condensation coefficient is small (e.g., 0.1), it does not affect the results.

Time scale τ_3 can be estimated assuming that hibonite overgrowths formed by reaction between corundum condensates and nebular gas, which is controlled by calcium diffusion in corundum. Because almost all aluminum (≥95%) in a solar nebula at total pressures of 10^{-6}–10^{-5} atm condenses as corundum prior to formation of hibonite (Yoneda and Grossman 1995), only a small amount of hibonite might have condensed directly from a nebular gas. In corundum aggregate #2-11, no hibonite overgrowths were detected,

suggesting that direct condensation of hibonite from the gas did not occur. This could be due to 1) very rapid cooling of the nebular region, 2) a subsolar Ca/Al ratio of the nebular gas, 3) quick removal of corundum from the high temperature region, or 4) the presence of undetected hibonite. We neglect direct condensation of hibonite and consider τ_3 as the time over which calcium diffuses inward from the surface of corundum grains (0.1 μm in the case of #2-11). Since Ca diffusion in corundum is expected to be a slow process (see below), this gives an upper limit to the time scale of hibonite formation. We may also need to consider the time required for calcium diffusion through any hibonite layer formed by replacement of corundum. Diffusion rates of calcium in hibonite are not known. In general, diffusion rates in minerals depend on physical properties of minerals (Watson and Baxter 2007) such as melting points and hardness. Corundum is known to have a high melting point and high hardness. Therefore, it is unlikely that diffusion rates in hibonite are slower than in corundum. Thus, this process is neglected.

The diffusion rate of calcium in corundum is also unknown and we have to make a crude estimate. Aluminum self-diffusion rates, D_{Al} (cm²/s), in a single crystal of α-Al_2O_3 (Le Gall et al. 1994) are $D_{Al} = 0.16 \ exp(-510 \ (kJ/mol)/RT)$. Since diffusion rates of divalent atoms in corundum are faster than that of aluminum (e.g., nickel diffusion rate is about 100 times faster than that of aluminum [Le Gall et al. 1994]), the calcium diffusion rates D_{Ca} in corundum are assumed to be 1–10 times that of aluminum. (Because of the large ionic radius of calcium, its diffusion rate is probably smaller than that of nickel.) Using the relationship $t \sim x^2/D_{Ca}$, where x is distance and t is time, a time scale for the formation of hibonite overgrowths can be estimated.

Our estimate of the time scale for the formation of a layer of hibonite 0.1 μm thick by replacement of corundum (the sum of τ_1, τ_2, τ_3; where τ_2 generally is much smaller than τ_1 or τ_3) is illustrated in Fig. 7. The pressure dependence in Fig. 7 is mostly due to the pressure dependence of the hibonite equilibrium condensation temperature: at high pressures, the hibonite condensation temperature is high and calcium diffusion is quick, resulting in small values of τ_3. For a corundum grain 10 μm in size and fast calcium diffusion rate ($D_{Ca} \sim 10 \times D_{Al}$), τ_1 and τ_3 are comparable, and the total times for hibonite formation are 2.4×10^8 and 1.6×10^7 s at 10^{-6} atm and 10^{-5} atm, respectively. At slower calcium diffusion rates (e.g., $D_{Ca} \sim D_{Al}$), τ_3 becomes the dominant factor, and the time scale for the formation of a hibonite overgrowth around a 10 μm size corundum grain are 7.3×10^8 and 7.9×10^7 s at 10^{-6} atm and 10^{-5} atm, respectively.

Relative Velocities between Corundum Grains and Time Scale for the Formation of Corundum Aggregates

Assuming that the sticking probability between colliding grains is 1 for slow collisions (i.e., below the critical velocity for sticking, V_{St}, [Chokshi et al. 1993]), their accretion time

scale (t_{acc}) can be expressed as $t_{acc} = 1/(n\sigma\Delta V_{rel})$, where n is the number density of grains, and ΔV_{rel} is the relative velocity. The collisional cross section σ is calculated as $\pi (r_1 + r_2)^2$, where r_1 and r_2 are radii of two colliding grains. The number density of corundum grains is expressed as $n = \zeta\rho_g/m_d$, where ζ is the mass fraction of corundum grains, ρ_g is the total density of the nebular region, and m_d is the mean mass of corundum grains.

To explain the presence of the hibonite-free corundum aggregates, the collision time scale of corundum grains has to be shorter than the hibonite formation time scale. Using this requirement, we can estimate the relative velocity (V_{req}) between corundum grains. It is proportional to the grain size and nearly independent of the total pressure. For corundum grains 10 μm in size ($r = 5$ μm), V_{req} is ~5×10^2 cm/s at 10^{-6} atm. This was obtained for an assumed hibonite thickness of 0.1 μm. It is inversely proportional to the square of the assumed hibonite thickness.

Relative velocities between grains in the solar nebula are considered to have been produced by several mechanisms: Brownian motion (V_B), sedimentation toward the equatorial plane due to the vertical component of the solar gravity (V_S), turbulent motion (V_T), and photophoresis (V_P). An additional requirement is that the relative velocity has to be smaller than V_{St}. In our analysis, relative velocities between grains of slightly different (by 20%) radii were calculated, and the formation region of the corundum-bearing grains was assumed to be close to the protosun (0.06 AU) (e.g., Shu et al. 1996). To estimate the effect of the distance from the protosun, calculations were also made at 2.7 AU. We note, however, that the high temperatures required to condense corundum and hibonite (~1500 K at 10^{-6} atm) are not expected at 2.7 AU in the canonical solar nebula model (e.g., Nakagawa et al. 1981) assumed in our calculations (see Cassen [2001] for an opposing view).

Brownian Motion

Dust grains in the protoplanetary disk are in Brownian motion and collide mutually with a relative velocity that can be expressed as $V_B = (8kT/\pi)^{1/2} \times (1/m_1+1/m_2)^{1/2}$, where m_1 and m_2 are masses of the colliding dust grains, k is the Boltzmann's constant, and T is the temperature of the nebular gas (Nakagawa et al. 1981). It is estimated that V_B is less than 1 cm/s and, therefore, can be neglected.

Sedimentation Due to the Vertical Component of the Solar Gravity

When the solar nebula reaches a thermally steady, hydrostatic equilibrium state, where turbulent motions have already decayed, dust grains floating in the solar nebula began to sink toward its equatorial plane due to the vertical component of the solar gravity. The vertical motion of a spherical dust grain of radius r and density ρ_d can be

described as $dV_Z/dt = - (\rho_g/\rho_d)(C_t/r)V_Z - (GM_{Sun}/R^3)Z$, where V_Z is the grain's vertical velocity in a gas of density ρ_g, C_t is the mean thermal velocity of gas molecules, Z is the height from the equatorial plane, and G, M_{Sun}, and R denote the gravitational constant, the solar mass, and the distance from the Sun, respectively (Nakagawa et al. 1981). In this nebula model, the dust grains always sink with a terminal velocity given by $V_Z = (\rho_d/\rho_g)(r/C_t)(GM_{Sun}/R^3)Z$. Dust grains having different radii, r_1 and r_2, which are at the same height, Z, above the equatorial plane, will collide with a relative velocity $V_S = (\rho_d/\rho_g C_t)(GM_{Sun}/R^3)Z|r_1 - r_2|$. We calculated relative velocities due to sedimentation at the scale height Z_H of the nebula. According to Nakagawa et al. (1981), $Z_H \sim C_t/\Omega$, where Ω is the orbital frequency of the Keplerian motion. The relative velocity between dust grains due to sedimentation is smaller farther away from the Sun. For grains 10 μm in size, at 0.06 AU and 10^{-6} atm, V_S is ~210 cm/s; it is proportional to the grain size and inversely proportional to the total pressure.

Turbulent Motion

The turbulent velocity, V_T, associated with the largest eddies, is generally assumed to be proportional to the sound speed c. Here we use the α model, which assumes $V_T \sim \alpha c$. The earlier estimates of the α value range from 0.1 (Morfill 1983) to 0.3 (Morfill et al. 1985); more recent estimates of α range from 3×10^{-4} to 3×10^{-3} (Cuzzi et al. 2003). In our calculations, we used $V_T \sim 0.3c$, representing a plausible upper limit for turbulent velocities in the accretionary disk.

The properties of turbulence in the solar nebula are usually constrained by dimensional arguments. The turbulence is assumed to have a power-law autocorrelation spectrum spanning a range of wavenumbers from k_0, associated with large eddies, to k_s for the smallest. The largest eddies have maximum length scale of the order of the disk thickness Z_H, whereas the system's rotation tends to impose a characteristic time scale $t_{k0} \sim 1/\Omega$ for their convective overturn (Tennekes and Lumley 1972). For a Kolmogorov turbulence spectrum, the largest eddies supply energy to smaller ones, which drive still smaller ones, and so on. This cascade extends down to a limiting eddy size at which viscous dissipation becomes important. From dimensional arguments (Tennekes and Lumley 1972), the rate at which the largest eddies supply kinetic energy (per unit mass) is $\varepsilon \sim V_T^3 /Z_H$, which must be equal to the mean rate of viscous dissipation in the smallest eddies. This consideration defines the so-called "inner scales" associated with the smallest eddies: length $l \sim (v^3/\varepsilon)^{1/4}$, velocity $u \sim (v\varepsilon)^{1/4}$, and time $t_{ks} \sim (v/\varepsilon)^{1/2}$, where v is the (molecular) kinematic viscosity of the gas and t_{ks} is a turn over time scale for the smallest eddies (Weidenschilling 1984).

For small (<100 μm) grains of radii r_1 and r_2, $V_T = (t_2 - t_1) (u/t_{ks})$. Here, t_1 and t_2 are the stopping time by the gas, which can be expressed as $t_1, t_2 = (r_1, r_2)\rho_d/(C_t\rho_g)$. For grains 10 μm

in size at 0.06 AU and 10^{-6} atm, $V_T \sim 2.8 \times 10^3$ cm/s. We note that this is the upper limit because α is assumed to be $\sim$0.3. At large distances from the Sun, the disk thickness is large and, hence, ε is small; therefore, the velocity of the smallest eddies and V_T are small.

Drift Velocity Due to Photophoresis

Photophoresis effects on dust particles irradiated by the central star in a gaseous nebula have recently been proposed as the dominant mechanism for moving dust particles in the solar nebula (Krauss and Wurm 2005; Wurm and Krauss 2006). According to this mechanism, the side of a particle facing the Sun is at a higher temperature than its opposite side. Since gas molecules leave the Sun-facing grain surface at higher velocities than they leave the shaded side, the dust particles are propelled away from the Sun. The photophoresis drift velocity is proportional to the grain size and solar irradiation, and inversely proportional to the thermal conductivity of the particle and the thermal velocity of the gas molecules; it is independent of the nebula pressure (Wurm and Krauss 2006). At early stages of protoplanetary disk evolution, the nebula is largely opaque to solar irradiation, and photophoresis is inefficient. Therefore, Wurm and Krauss (2006) suggested that photophoresis was important only for the late-stage protoplanetary disk, when it became transparent up to several AU. However, corundum is probably one of the earliest and highest temperature solar nebula condensates, and probably formed near the Sun. As a result, corundum grains are likely to have been irradiated by the Sun during condensation and aggregation. Using Equation 7 of Wurm and Krauss (2006), a photophoresis drift velocity of $\sim$10 cm/s is obtained for a corundum grain 10 μm in size at $\sim$0.06 AU for a nominal solar luminosity, using a typical thermal conductivity of $\sim$5 Wm^{-1}K^{-1} at 1500 K. At this grain size, the drift velocity due to solar radiation pressure (momentum given by photons) is of a magnitude similar to that due to the photophoresis. But the drift velocity due to radiation pressure is independent of grain size and does not cause collisions between the grains (Takeuchi and Artymowicz 2001). In contrast, photophoresis is proportional to the size and results in collisions between grains of different sizes. Assuming a 20% difference in radii of grains of $\sim$10 μm in size, we obtain a relative velocity of $\sim$2 cm/s. This velocity is low compared with other velocities, e.g., due to turbulence. However, the early Sun may have been much more luminous than it is now. For example, luminosity of solar mass stars during FU Orionis events could be as high as 100–1000 times that of the present solar luminosity (3.85×10^{26} W). Therefore, if the early Sun was very luminous, photophoresis could have resulted in relative velocities >200 cm/s. Because V_P is independent of gas pressure, as opposed to V_S and V_T, it is, in a relative sense, more effective at higher pressures.

Velocity Upper Limit for Sticking

Depending on the relative velocity and material parameters, two colliding dust particles can stick, bounce, fragment, melt, or vaporize upon collision. V_{St} is the highest velocity for which sticking between grains occurs and depends on the size, elastic properties, and surface energy of the grains. Chokshi et al. (1993) showed that $V_{St} \sim 3.86\ \gamma^{5/6}/(E^{1/3}r^{5/6}\rho_d^{1/2})$, where E is the Young's modulus and γ is the surface energy of the chemically identical grains. Material with a smaller E will stick better because it will more readily deform, leading to a larger contact area. Similarly, a larger γ will lead to increased binding across the contact area and, therefore, to increased V_{St}. The critical velocity decreases with increasing sizes (r) of the colliding grains. Assuming $\gamma = 690$ erg/cm^2, $E = 4 \times 10^{12}$ dyn/cm^2, and $\rho_d = 4.0$ g/cm^3, for 1 μm and 10 μm size corundum grains, V_{St} are estimated to be $\sim$110 cm/s and $\sim$16 cm/s, respectively.

Formation of Corundum Aggregates in the Nominal Solar Nebula

Various velocities (V_B, V_P, V_S, V_{St}, V_T, and V_{req}) for 1 μm and 10 μm size grains at 0.06 AU and for 10 μm size grains at 2.7 AU are plotted in Fig. 8. The necessary conditions for the formation of corundum aggregates are 1) the critical velocity for sticking V_{St} should be larger than the required velocity V_{req} for aggregate formation, and 2) at least one of the relative velocities (e.g., V_S) should be between V_{St} and V_{req}. In Fig. 8, the calcium diffusion rate in corundum D_{Ca} is assumed to be equal to the aluminum diffusion rate D_{Al}, which gives the slowest V_{req}. The relative velocity due to turbulence V_T is an upper limit because $\alpha \sim 0.3$ is assumed. The sedimentation velocity V_S is assessed at the nebula scale height and could be smaller at lower heights. The relative velocity due to photophoresis V_P is calculated for the present solar luminosity and could be larger (about 100 times) if the early Sun were more luminous.

V_S and V_T decrease with increasing pressure, because dust grains are dragged more strongly at higher pressures. In contrast, V_B, V_P, V_{St}, and V_{req} show no strong dependence on the nebular pressure. V_B and V_P are small and generally much smaller than V_{req} for the formation of corundum aggregates.

For 1 μm size grains (Fig. 8a), V_{req} and V_{St} are of similar magnitude; V_T could also be of a similar magnitude if an appropriate α value is chosen for V_T. This means that aggregate formation may be possible. We note, however, that Fig. 8a shows the optimal case for aggregate formation since V_T is assumed to be large ($\alpha \sim 0.3$) and the hibonite formation is slow ($D_{Ca} \sim D_{Al}$). If $D_{Ca} \sim 10 \times D_{Al}$, then V_{req} is about ten times faster, and the presence of the apparently hibonite-free corundum aggregates is difficult to explain in the canonical solar nebula that cools at a steady rate. For grains 10 μm in size (Fig. 8b), V_{req} is higher than V_{St}. Therefore, our calculations indicate that formation of corundum aggregates
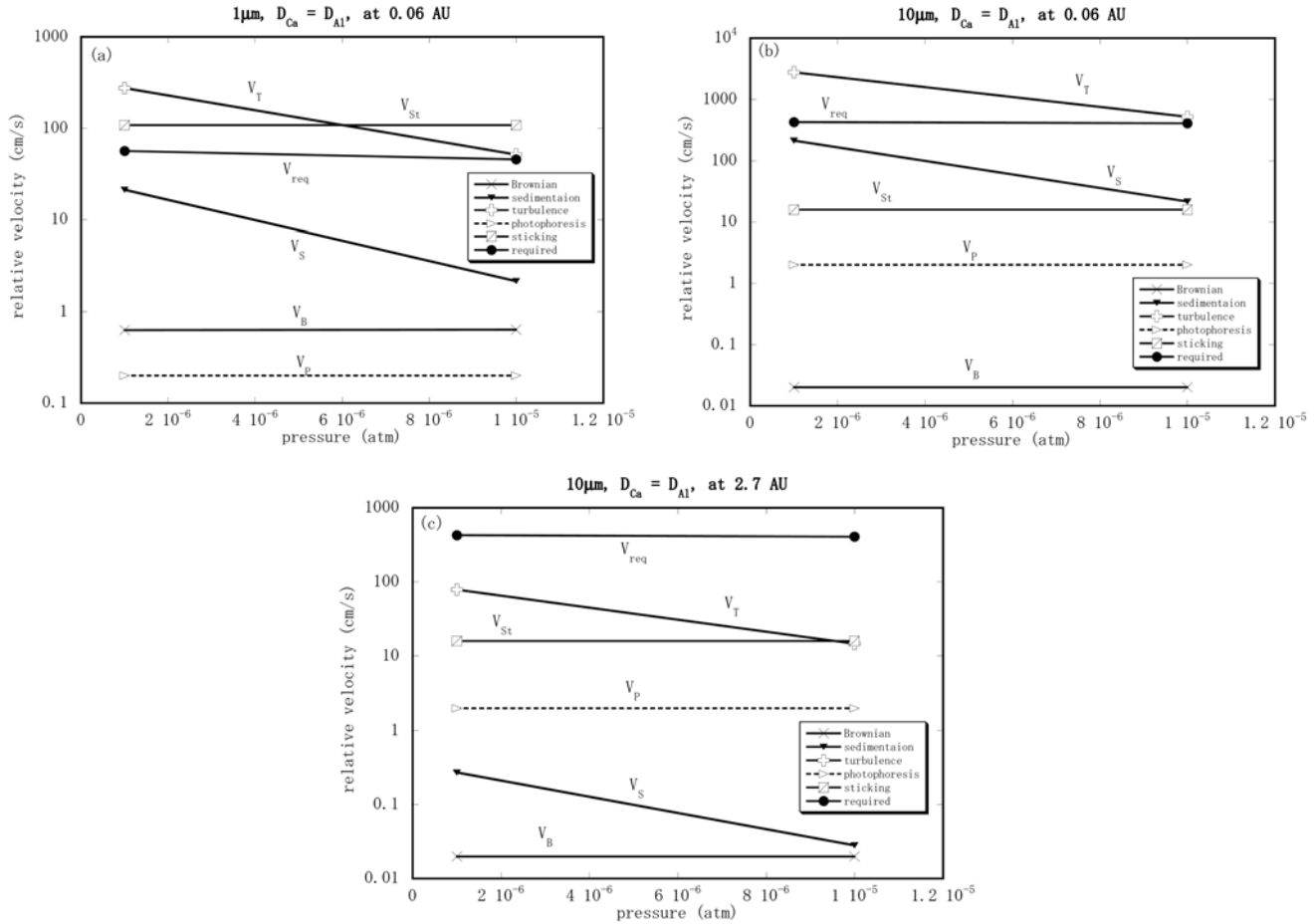
Fig. 8. Relative velocities between corundum grains shown as a function of total nebula pressures with slow Ca diffusion in corundum. About 20% difference in the radius is assumed. a) For 1 μm size grains at 0.06 AU, the critical velocity for sticking is higher than the velocity required for aggregate formation. Turbulence could provide sufficient relative velocity for aggregate formation. b) For 10 μm size grains at 0.06 AU, the critical velocity for sticking is lower than the velocity required for aggregate formation, suggesting that aggregate formation in the nominal solar nebula is unlikely. c) At 2.7 AU, relative velocities due to turbulence and sedimentation are much lower than those at 0.06 AU; other relative velocities remain unchanged. This indicates that aggregate formation is difficult at 2.7 AU.

is impossible in the nominal solar nebula that cools at a steady rate.

At 2.7 AU, V_S and V_T are both more than one order of magnitude smaller compared with those at 0.06 AU. The other relative velocities are independent on the distance from the Sun. In the nebula model of Nakagawa et al. (1981), both temperature and pressure are determined by the distance from the Sun and the height from the mid-plane. Such explicit dependence of these parameters on the location in the nebula is ignored in our calculations. Pressure is considered as a free parameter and temperature is determined by the condensation temperatures of corundum and hibonite. The Sun's gravity, which directly affects V_S, is the only factor that depends on the distance from the Sun. It also affects V_T through the scale height of the nebula. In any case, at 2.7 AU, none of the relative velocities are higher than V_{req} for grains 10 μm in size. Also, V_{req} for grains 10 μm in size is higher than V_{St}, suggesting that formation of corundum aggregates at 2.7 AU is unlikely.

Other Possibilities

Here we discuss several other possible environments for the formation of corundum aggregates, including 1) dust-enriched nebular region, 2) long residence time of corundum grains in a nebular region with ambient temperature between condensation temperatures of corundum and hibonite, 3) chemically fractionated (calcium-poor) nebula, and 4) heterogeneous condensation of corundum.

Dust-Enriched Solar Nebula

If we assume that aggregates of corundum grains formed in a hot, dust-enriched nebular region, the number density of corundum grains will be larger than that in the nominal solar nebula and the time scale of aggregate formation is expected to be shorter. However, the condensation temperatures of corundum and hibonite are higher in the dust-enriched nebula, and the difference in the condensation temperature of

corundum and hibonite is smaller (Ebel and Grossman 2000; Ebel 2006). As a result, calcium diffusion in corundum is expected to be faster and formation of hibonite to be quicker, whereas the relative velocity required for the formation of the corundum aggregates is only slightly reduced (~5%) in a nebula with 10 times the dust enrichment compared with that in the nominal solar nebula. Because of these side effects, V_{req} remains higher than V_{St}, suggesting that formation of corundum aggregates will be difficult under such conditions. Although in the equatorial plane of a non-turbulent nebula, dust is expected to be enriched by sedimentation, such sedimentation takes more than 10^3 years for grains 10 μm in size in the nominal solar nebula (Nakagawa et al. 1981), which is inconsistent with the time constraints on the formation of corundum aggregates discussed above based on the homogeneous nucleation theory.

Long Residence Time of Corundum Grains in a High Temperature Nebular Region

If, after condensation, corundum grains stayed in a nebular region with ambient temperature above the condensation temperature of hibonite for a long time, the hibonite-free corundum aggregates could have formed (subsequent isolation of such grains from this region is still required). The cooling history of the nebular region might be recorded in a sintering (annealing) state of the corundum-bearing aggregates. Sintering is driven to reduce the surface energy at the neck (contact area) of two grains. The time and size dependence of sintering of two spherical grains of corundum were given by Coble (1958) as $x/r = (40\gamma a^3 D*/kT)^{1/5} r^{-3/5} t^{1/5}$, where x (cm) is the neck size, r (cm) is the radius of a sphere, $D*$ (~3×10^{-16} cm^2/s at ~1510 K, ~5×10^{-15} cm^2/s at 1580 K) is an apparent self-diffusion coefficient, γ (690 erg/cm^2) is the surface energy of corundum, and a^3 is the volume of a vacancy in the Al_2O_3 lattice, which is assumed to be 1.4×10^{-23} cm^3.

Sintering time scales for ($x/r \sim 0.5$) for corundum grains 10 μm in size at the condensation temperature of corundum in a nebular region at 10^{-6} atm (~1510 K) and 10^{-5} atm (~1580 K) are calculated as 7×10^9 s and 4×10^8 s, respectively, which are much longer than the time scale for cooling nebular gas from corundum condensation temperature to hibonite condensation temperature (Watanabe et al. 1990). The poorly sintered nature of aggregate #2-11 is consistent with these calculations. Therefore, a high-temperature nebula that stays above the condensation temperature of hibonite is a possible environment for the formation of corundum aggregate #2-11. The inner edge of the solar nebula is a possible location that could keep such high temperatures for a long time.

We note that the long time scale required for sintering corundum grains suggests that grains 10 μm in size (except the one made of two subgrains) in aggregate #2-11 formed as single crystals rather than as an aggregate of smaller grains that later experienced coarsening by sintering.

Chemically Fractionated (Calcium-Poor) Nebula

If the nebular region was chemically fractionated (calcium-poor), hibonite formation would be delayed and the presence of the hibonite-free corundum aggregates can be easily explained. Transport of grains is expected to be vigorous at the inner edge of the solar nebula (e.g., Takeuchi and Lin 2003). If corundum grains were transported across a corundum condensation front, chemical fractionation might occur (e.g., Cuzzi and Zahnle 2004), making the inner region enriched in more refractory elements. In this context, aluminum might be enriched relative to calcium in the inner edge of the protoplanetary disk. Based on the pressure dependence of condensation temperature of hibonite (Yoneda and Grossman 1995), depletion in calcium by a factor of about 3 would lower the condensation temperature of hibonite by ~40 K, which is significant, because in our calculations the difference in condensation temperatures of corundum and hibonite is ~30 K at 10^{-6} atm and ~6 K at 10^{-5} atm.

Heterogeneous Condensation of Corundum

The homogeneous condensation of corundum discussed above is considered to be likely mainly based on the similarity of the constituent grain size in an aggregate. However, heterogeneous condensation of corundum cannot be ruled out completely and we need to evaluate its plausibility as well.

Heterogeneous condensation of corundum grains requires the presence of seeds; if such seeds were present, they were most likely pre-existing corundum grains that could have formed as evaporation residues during a large-scale, high-temperature heating event similar to those that result in the formation of type B CAIs. In this case, the condensation temperature of corundum is the same as its equilibrium condensation temperature. Grain sizes of the newly formed corundum grains will be inversely proportional to the number of pre-existing seeds. With equilibrium condensation, corundum is stable over a temperature range of ~90 K at 10^{-6} atm (Yoneda and Grossman 1995). This is about three times larger than in the case of homogeneous condensation, favoring formation of corundum aggregates. However, if the pre-existing seed crystals were not vaporized completely, the duration of heating events was short, and the cooling rate was likely to be fast. If this thermal event was similar to the events that melted type B CAIs in CV chondrites, then the cooling rate is ~2 orders of magnitude faster than that postulated for the homogeneous condensation. The corresponding cooling time is ~10^5–10^7 s (see the Grain Size and Cooling Time According to a Homogenous Nucleation Theory section). The accretion time scale (see the Relative Velocities between Corundum Grains and Time Scale for the Formation of Corundum Aggregates section) of corundum grains 10 μm in size is ~2.1×10^9 s at 10^{-5} atm assuming that the relative velocity is equal to the critical velocity for sticking. Therefore, we conclude that heterogeneous condensation is not a viable mechanism for the origin of corundum aggregates, if the heating-cooling event was similar to those
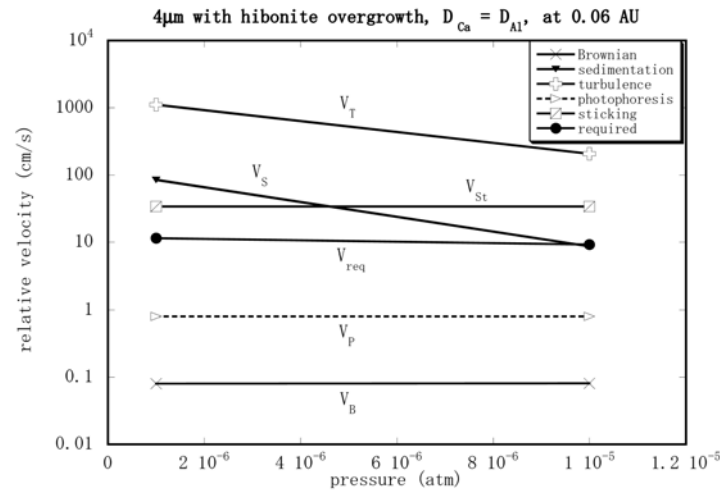
Fig. 9. Relative velocities between corundum grains 4 μm in size with a 0.5 μm thick hibonite overgrowth at 0.06 AU in the case of slow Ca diffusion in corundum ($D_{Ca} = D_{Al}$). About 20% difference in the radius is assumed. The critical velocity for sticking is higher than the required velocity of aggregate formation. Both turbulence and sedimentation could provide sufficient relative velocities for aggregate formation. If the luminosity of the early Sun was more than ten times higher than its present luminosity, photophoresis could have provided sufficient relative velocity for aggregate formation. Physical properties of hibonite are assumed to be similar to those of corundum.

that formed CAIs. If, however, the heating-cooling process were a very slow one (~10^9 s), comparable with the time scale deduced from the aggregate formation, then heterogeneous condensation may be a viable mechanism.

Corundum Aggregate with Thick Hibonite Overgrowths

Here we examine the time scale for the formation of a hibonite-bearing corundum aggregate (~4 μm in size with a hibonite layer of ~0.5 μm in thickness; see #2-23 in Fig. 2c). The procedure is similar to that used for the aggregation of hibonite-free corundum aggregates. It is not possible to know based on the petrographic evidence if the aggregate formed before hibonite formation or the aggregate formed after hibonite formation. However, the plausibility of the former process can be examined based on the discussion on corundum aggregate formation. The grain size (~4 μm) of aggregate #2-23 is intermediate between 1 μm (Fig. 8a) and 10 μm (Fig. 8b). Examination of these figures shows that aggregation of hibonite-free corundum (4 μm in size) does not occur in the steadily cooling nominal solar nebula. Therefore, in the following we assume that aggregation occurred after hibonite formation. This means that the collision time scale of the constituent grains was longer than the formation time scale of the 0.5 μm thick hibonite overgrowth. From this requirement, the collision velocity required for the formation of corundum with hibonite overgrowth (V_{req}) was obtained and compared with other velocities in Fig. 9.

In the case of $D_{Ca} = D_{Al}$ at 10^{-6} atm, V_{req} is slightly smaller than V_{St}; it is also smaller than V_S and V_T. V_T shown in Fig. 9 is the upper limit; V_S is assessed at the nebula scale height and could be smaller near the equatorial plane.

Therefore, in this case, hibonite-bearing corundum aggregates may form in the nominal solar nebula that cools at a steady rate. The nebula cooling rate that produces corundum grains 4 μm in size is ~7×10^{-9} K/s, which is about three times faster than the cooling rate that produces grains 10 μm in size. At this cooling rate, hibonite is stable for ~10^{10} s, from 1485 K to 1286 K, at which temperature it is replaced by spinel. This time scale is comparable with that for forming 0.5 μm thick hibonite from corundum by calcium diffusion at a diffusion rate $D_{Ca} \sim D_{Al}$. Therefore, the aggregate of corundum with hibonite overgrowth may be considered a product of a nebula that cooled slowly from 1500 K to 1300 K. Three corundum-hibonite grains in aggregate #2-23 (Fig. 2c) are well-sintered. Although sintering rates of hibonite grains are not known, since the melting temperature of hibonite is significantly lower (though it is incongruent melting) than that of corundum, diffusion (and hence sintering) rates in hibonite are expected to be faster than that in corundum. Therefore, the well-sintered appearance of #2-23 may not require exceedingly slow cooling. The aggregate #2-23 seems to have cooled at a faster rate and to a lower temperature than the apparently hibonite-free corundum aggregate #2-11. As discussed earlier, the formation location of #2-11 is considered to be very close to the Sun. The formation location of #2-23 was probably farther away from the Sun where the temperature was lower than the hibonite condensation temperature due to higher opacity of the nebula. However, it has to be fairly close to the x-point if the aggregate was blown away by an X-wind (Shu et al. 1996). Future studies of hibonite formation kinetics and hibonite sintering will remove uncertainties of the present discussion and contribute significantly to understanding of accretion processes in the high temperature regions of the solar nebula.

CONCLUSIONS

Corundum and corundum-hibonite grains and their aggregates composed of two to six grains of similar sizes, which appear to have retained evidence for condensation and accretion processes in high-temperature regions of the early solar system, were found in the Acfer 094 matrix. The abundance of the corundum-bearing grains is estimated to be ~8 ppm relative to the matrix fraction.

We estimated formation time scales of aggregates of corundum grains 1 to 10 μm in size and an aggregate of corundum-hibonite grains 4 μm in size based on a homogeneous nucleation theory and hibonite formation that is controlled by calcium diffusion in corundum. From this time scale, relative velocities between grains were estimated and compared with various velocities in the solar nebula. We conclude that formation of corundum aggregates composed of grains 10 μm in size is difficult in the nominal steadily cooling solar nebula. Our calculations suggest instead that there are two possible scenarios for the formation of the corundum aggregates: i) a hot nebular region close to the Sun where the ambient temperature was kept between condensation temperatures of corundum and hibonite for a long time, and ii) cooling in a chemically fractionated (calcium-depleted) nebular region. The hibonite-bearing corundum aggregates could have formed naturally in a steadily cooling, nominal solar nebula.

We suggest that the formation region of the corundum and corundum-hibonite grains is closer to the Sun compared with normal CAIs. This is based on both the very refractory nature of the constituent minerals and the presence of aggregates with large (10 μm in size) constituent grains. The former is explained by removal at higher temperatures than those of normal CAIs. But the latter cannot be explained easily in the formation region of normal CAIs.

Editorial Handling—Dr. Larry Nittler

REFERENCES

Bar-Matthews M., Hutcheon I. D., MacPherson G. J., and Grossman L. 1982. A corundum-rich inclusion in the Murchison meteorite. *Geochimica et Cosmochimica Acta* 46:31–41.

Bischoff A. and Geiger T. 1994. The unique carbonaceous chondrite Acfer 094: The first CM3 chondrite (?) (abstract). 25th Lunar and Planetary Science Conference. pp. 115–116.

Bland P. A., Rost D., Vicenzi E. P., Stadermann F. J., Floss C., Fries M., Steele A., Benedix G. K., Lee M. R., Watt L. E., and Kearsley A. T. 2005. Trace element carrier phases in primitive chondrite matrix: Implications for volatile element fractionation in the inner solar system (abstract #1841). 36th Lunar and Planetary Science Conference. CD-ROM.

Bland P. A., Stardermann F. J., Floss C., Rost D., Vicenzi E. P., Kearsley A. T., and Benedix G. K. 2007. A cornucopia of presolar and early solar system materials at the micrometer size range in primitive chondrite matrix. *Meteoritics & Planetary Science* 42. This issue.

Blander M. and Katz J. L. 1967. Condensation of primordial dust. *Geochimica et Cosmochimica Acta* 31:1025–1034.

Cassen P. 2001. Nebular thermal evolution and the properties of primitive planetary materials. *Meteoritics & Planetary Science* 36:671–700.

Chokshi A., Tielens A. G. G. M., and Hollenbach D. 1993. Dust coagulation. *The Astrophysical Journal* 407:806–819.

Coble R. L. 1958. Initial sintering of alumina and hematite. *Journal of the American Ceramic Society* 41:55–62.

Cuzzi J. N., Davis S. S., and Dobrovolskis A. R. 2003. Blowing in the wind. II—Creation and redistribution of refractory inclusions in a turbulent protoplanetary nebula. *Icarus* 166:385–402.

Cuzzi J. N. and Zahnle K. J. 2004. Material enhancement in protoplanetary nebulae by particle drift through evaporation fronts. *The Astrophysical Journal* 614:490–496.

Ebel D. S. and Grossman L. 2000. Condensation in dust enriched systems. *Geochimica et Cosmochimica Acta* 64:339–366.

Ebel D. S. 2006. Condensation of rocky material in astrophysical environments. In *Meteorites and the early solar system II*, edited by Lauretta D. and McSween H. Y., Jr. Tucson, Arizona: The University of Arizona Press. pp. 253–277.

Fahey A. J. 1988. Ion microprobe measurements of Mg, Ca, Ti, and Fe isotopic ratios and trace element abundances in hibonite-bearing inclusions from primitive meteorites. Ph.D. thesis, Washington University, Saint Louis, Missouri, USA. 232 p.

Gao X., Amari S., Messenger S., Nittler L. R., Swan P. D., and Walker R. M. 1996. Survey of circumstellar grains in the unique carbonaceous chondrite Acfer 094 (abstract). *Meteoritics & Planetary Science* 31:A48.

Greshake A. 1997. The primitive matrix components of the unique carbonaceous chondrite Acfer 094: A TEM study. *Geochimica et Cosmochimica Acta* 61:437–452.

Grossman J. N. and Brearley A. J. 2005. The onset of metamorphism in ordinary and carbonaceous chondrites. *Meteoritics & Planetary Science* 40:87–122.

Hinton R. W., Davis A. M., Scatena-Wachel D. E., Grossman L., and Draus R. J. 1988. A chemical and isotopic study of hibonite-rich refractory inclusions in primitive meteorites. *Geochimica et Cosmochimica Acta* 52:2573–2598.

Ireland T. R. 1988. Correlated morphological, chemical, and isotopic characteristics of hibonites from the Murchison carbonaceous chondrite. *Geochimica et Cosmochimica Acta* 52:2827–2839.

Kimura M., Weisberg M. K., and Grossman J. N. 2006. Fe-Ni metal and sulfides in Acfer 094: Thermal history of the most primitive chondrite (abstract). *Meteoritics & Planetary Science* 41:A96.

Kozasa T. and Hasegawa H. 1987. Grain formation through nucleation process in astrophysical environments. *Progress of Theoretical Physics* 77:1402–1410.

Krauss O. and Wurm G. 2005. Photophoresis and the pile-up of dust in young circumstellar disks. *The Astrophysical Journal* 630: 1088–1092.

Krot A. N., Huss G. R., and Hutcheon I. D. 2001. Corundum-hibonite

refractory inclusions from Adelaide: Condensation or crystallization from melt (abstract)? *Meteoritics & Planetary Science* 36:A105.

Krot A. N., Fagan T. J., Keil K., McKeegan K. D., Sahijpal S., Hutcheon I. D., Petaev M. I., and Yurimoto H. 2004. Ca, Al-rich inclusions, amoeboid olivine aggregates, and Al-rich chondrules from the unique carbonaceous chondrite Acfer 094. I—Mineralogy and petrology. *Geochimica et Cosmochimica Acta* 68:2167–2184.

Le Gall M., Lesage B., and Bernardini J. 1994. Self-diffusion in α-Al$_2$O$_3$. I—Aluminium diffusion in a single crystals. *Philosophical Magazine A* 70:761–773.

Lin Y., Kimura M., Hiyagon H., and Monoi A. 2003. Unusually abundant refractory inclusions from Sahara 97159 (EH3): A comparative study with other groups of chondrites. *Geochimica et Cosmochimica Acta* 67:4935–4948.

MacPherson G. J., Grossman L., Hashimoto A., Bar-Matthews M., and Tanaka T. 1984a. Petrographic studies of refractory inclusions from the Murchison meteorite. Proceedings, 15th Lunar and Planetary Science Conference. pp. C299–C312.

MacPherson G. J., Paque J. M., Stolper E., and Grossman L. 1984b. The origin and significance of reverse zoning in melilite from Allende type B inclusions. *The Journal of Geology* 92:289–305.

MacPherson G. J., Davis A. M., and Zinner E. K. 1995. The distribution of aluminum-26 in the early solar system: A reappraisal. *Meteoritics* 30:365–386.

Morfill G. E. 1983. Some cosmochemical consequences of a turbulent protoplanetary cloud. *Icarus* 53:41–54.

Morfill G. E., Tscharnuter W., and Vork H. 1985. Dynamical and chemical evolution of the protoplanetary nebula. In *Protostars and planets II*, edited by Black D. Tucson, Arizona: The University of Arizona Press. pp. 493–533.

Mostefaoui S. and Hoppe P. 2004. Discovery of abundant in situ silicate and spinel grains from red giant stars in a primitive meteorite. *The Astrophysical Journal* 613:L149–L152.

Muzerolle J., D'Alessio P., Calvet N., and Hartmann L. 2004. Magnetospheres and disk accretion in Herbig Ae/Be stars. *The Astrophysical Journal* 617:406–417.

Nagashima K., Krot A. N., and Yurimoto H. 2004. Stardust silicates from primitive meteorites. *Nature* 428:921–924.

Nakagawa Y., Nakazawa K., and Hayashi C. 1981. Growth and sedimentation of dust grains in the primordial solar nebula. *Icarus* 45:517–528.

Nakamura T. M., Sugiura N., Kimura M., Miyazaki A., and Krot A. N. 2005. Corundum and corundum-hibonite grains discovered by cathodoluminescence in the matrix of Acfer 094 meteorite (abstract #1249). 36th Lunar and Planetary Science Conference. CD-ROM.

Nakamura T. M., Sugiura N., Kimura M., Miyazaki M., and Krot A. N. 2006. Condensation and accretion of corundum and corundum-hibonite grains in the solar nebula (abstract #1267). 37th Lunar and Planetary Science Conference. CD-ROM.

Newton J., Bischoff A., Arden J. W., Franchi I. A., Geiger T., Greshake A., and Pillinger C. T. 1995. Acfer 094, a uniquely

primitive carbonaceous chondrite from the Sahara. *Meteoritics* 30:47–56.

Nguyen A. N. and Zinner E. 2004. Discovery of ancient silicate stardust in a meteorite. *Science* 303:1496–1499.

Nittler L. R. 1997. Presolar oxide grains in meteorites. In *Astrophysical implications of the laboratory study of presolar materials*, edited by Bernatowicz T. J. and Zinner E. Woodbury, New York: American Institute of Physics. pp. 59–82.

Shu F. H., Shang H., and Lee T. 1996. Toward an astrophysical theory of chondrites. *Science* 271:1545–1552.

Simon S. B., Davis A. M., Grossman L., and McKeegan K. D. 2002. A hibonite-corundum inclusions from Murchison: A first-generation condensate from the solar nebula. *Meteoritics & Planetary Science* 37:533–548.

Spettel B., Palme H., Wlozka F., and Bischoff A. 1992. Chemical composition of carbonaceous chondrite from Sahara and Nullarbor Plains (abstract). *Meteoritics* 27:290–291.

Strebel R., Huth J., and Hoppe P. 2001. In situ location by cathodoluminescence and SIMS isotopic analyses of small corundum grains in the Krymka meteorite (abstract). 31st Lunar and Planetary Science Conference. pp. 1585–1586.

Sugiura N. 1998. Ion probe measurements of carbon and nitrogen in iron meteorites. *Meteoritics & Planetary Science* 33:393–409.

Takeuchi T. and Artymowicz P. 2001. Dust migration and morphology in optically thin circumstellar gas disks. *The Astrophysical Journal* 557:990–1006.

Takeuchi T. and Lin D. N. C. 2003. Surface flow in optically thick dusts by radiation pressure. *The Astrophysical Journal* 593:524–533.

Tennekes H. and Lumley J. L. 1972. *A first course in turbulence*. Cambridge, Massachusetts: MIT Press. 300 p.

Thrane K., Bizzarro M., and Baker J. 2006. Brief formation interval for calcium-aluminum-rich inclusions in the early solar system (abstract #1973). 37th Lunar and Planetary Science Conference. CD-ROM.

Watanabe S., Nakagawa Y., and Nakazawa K. 1990. Cooling and quasi-static contraction of primitive solar nebula after gas accretion. *The Astrophysical Journal* 358:282–292.

Watson E. B. and Baxter E. F. 2007. Diffusion in solid-Earth systems. *Earth and Planetary Science Letters* 253:307–327.

Weidenschilling S. J. 1984. Evolution of grains in a turbulent solar nebula. *Icarus* 60:553–567.

Wlotzka F. 1991. The Meteoritical Bulletin, No. 71. *Meteoritics* 26: 255–262.

Wurm G. and Krauss O. 2006. Concentration and sorting of chondrules and CAIs in the late solar nebula. *Icarus* 180:487–495.

Yoneda S. and Grossman L. 1995. Condensation of CaO-MgO-Al$_2$O$_3$-SiO$_2$ liquids from cosmic gases. *Geochimica et Cosmochimica Acta* 59:3413–3444.

Zinner E. K. 2003. Presolar grains. In *Meteorites, comets, and planets*, edited by Davis A. M. Treatise on Geochemistry, vol. 1. Oxford: Elsevier-Pergamon. pp. 17–39.